Conf-9111146--1

FAST-NEUTRON TOTAL AND SCATTERING CROSS SECTIONS OF ^{58}Ni AND NUCLEAR MODELS*

by

A. B. Smith, P. T. Guenther, J. F. Whalen, R. D. Lawson and S. Chiba+

Argonne National Laboratory

ANL/CP--73902

DE92 004000

SUMMARY

An extensive experimental and theoretical study of the fast-neutron interaction with ^{58}Ni was undertaken. The neutron total cross sections of ^{58}Ni were measured from ≈ 1 to > 10 MeV using white source techniques. Differential neutron elastic-scattering cross sections were measured from ≈ 4.5 to 10 MeV at ≈ 0.5 MeV intervals with ≥ 75 differential values per distribution. Differential neutron inelastic-scattering cross sections were measured, corresponding to fourteen levels with excitations up to ≈ 4.8 MeV. The measured results, combined with lower-energy values previously obtained at this laboratory and with relevant values available in the literature, were interpreted in terms of optical-statistical, dispersive-optical and coupled-channels models using both vibrational and rotational coupling schemes. The physical implications of the experimental results and their interpretation are discussed. The considerations are being extended to collective vibrational nuclei generally, exploring the potential for utilizing electro-magnetic matrix elements, deduced from experiment or predicted by the shell model, to determine the strengths of the neutron interaction. Detailed aspects of this work are given in the Laboratory Report, ANL/NDM-120 (in press).

---

* This work supported by the U. S. Department of Energy under contract No. W-31-109-ENG-38.

+ Visiting scientist from Japan Atomic Energy Research Institute, Tokai Establishment.

OBJECTIVES AND CONSIDERATIONS

It was the objective to provide comprehensive ^{58}Ni data for the design of fission and fusion energy systems by experimental and calculational means. Nickel is a primary constituent of most radiation-resistant ferrous alloys, and approximately 70% of the element consists of ^{58}Ni. In addition, the characteristics of the neutron interaction with ^{58}Ni are of fundamental interest as there are large direct-reaction components, and the isotope is a relatively simple nucleus consisting of a closed proton shell and two neutrons beyond a closed neutron shell.

A graded interpretation was followed, starting with a simple spherical optical-model interpretation providing a basis for many applications calculations. From this the effect of the dispersion relationship was explored, and then both vibrational and rotational coupling schemes were examined. A reasonable physical understanding of the neutron interaction was sought. Finally, some more fundamental aspects of the neutron interaction with collective nuclei were qualitatively examined with the objective of employing EM matrix elements and the shell model to calculate the neutron-induced processes.

MEASUREMENTS

The measurement regime extended to incident-neutron energies of > 10 MeV, and included detailed determinations of energy-averaged; i) total cross sections, ii) elastic-scattering cross sections, and iii) inelastic-scattering cross sections. The measurements were made in energy detail and with attention to accuracy so as to provide a quantitative data base consistency with the concepts of energy-averaged nuclear models. Detailed resonance behavior was intentionally energy averaged.

Mono-energetic and white source techniques were used to determine the total cross sections. The results are consistent with one another and with an equivalent energy average of the high-resolution total cross sections of Harvey [Har86], as illustrated in Fig. 1. This consistency implies no self-shielding distortions of the results.

Neutron elastic-scattering cross sections were determined with detailed energy and angle definition so as to provide a good energy-averaged data base for the model interpretations, as illustrated in Fig. 2. Particular attention was given to measurement accuracies and correction factors.

Cross sections for the inelastic-scattering excitation of 14 levels up to $E_x \approx 4.5$ were measured. A representative velocity spectrum obtained in the measurements is shown in Fig. 3. Most prominent of these inelastic cross sections are those due to the excitation of the first 1.454 (2^+) MeV vibrational level. At low

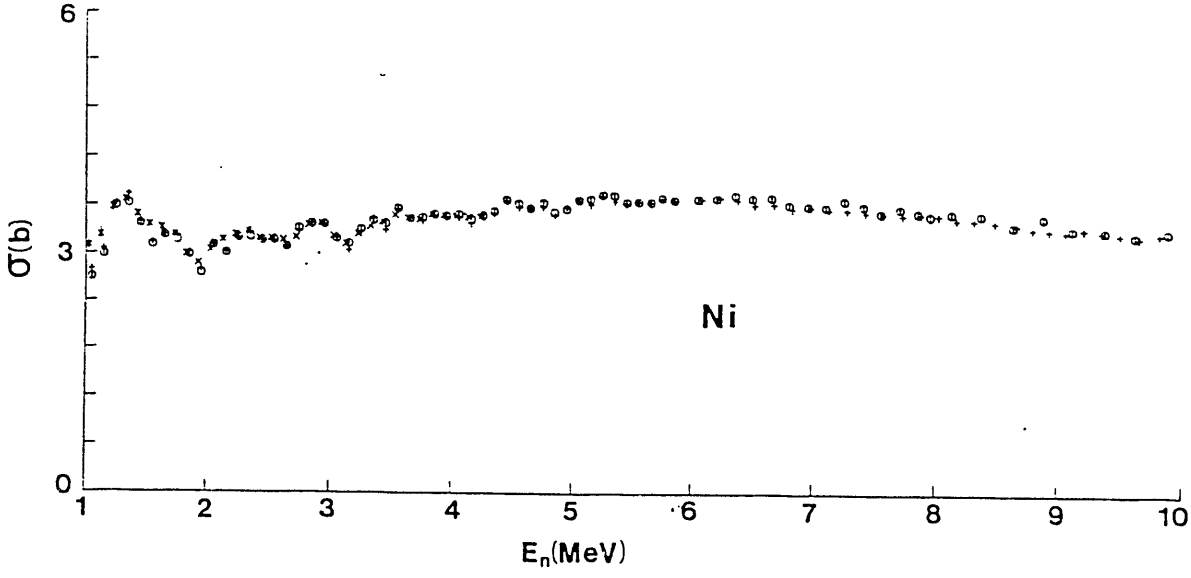

Fig. 1. Energy-averaged σ_t of ^{58}Ni. "0" = present work, "X" = Bud82, "+" = energy average of Har86.

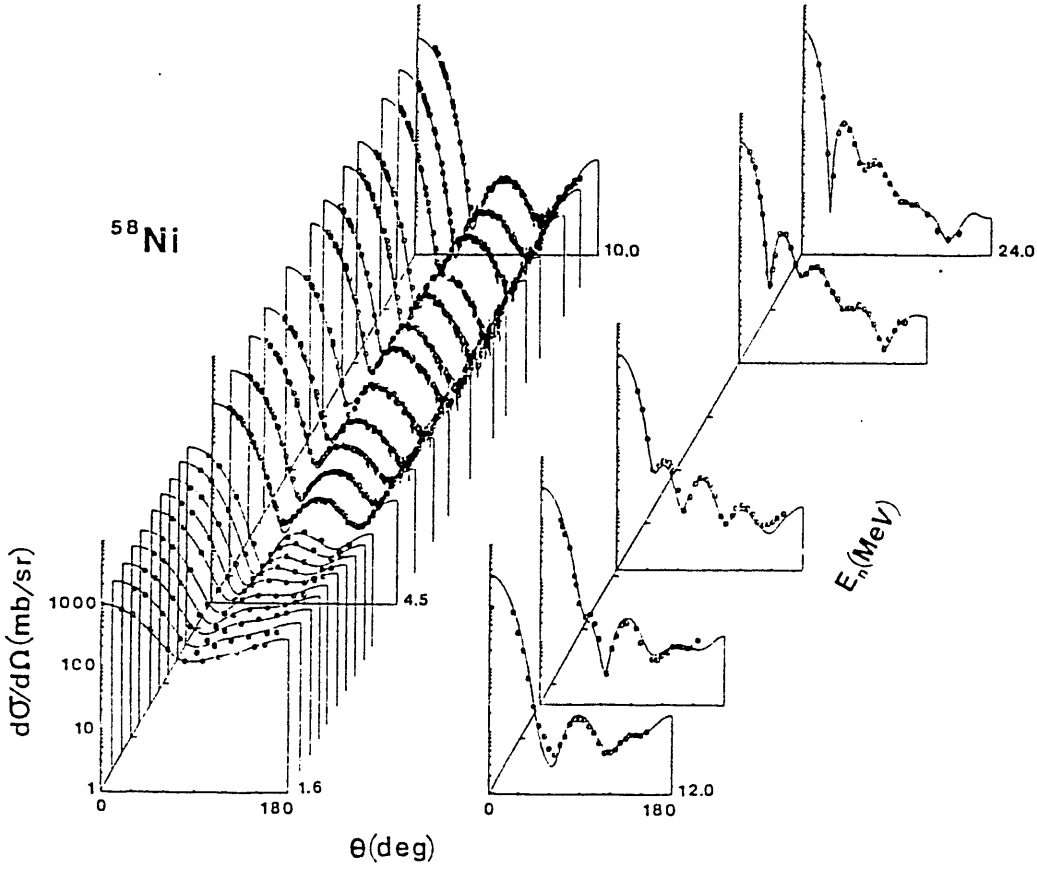

Fig. 2. Elastic scattering cross sections. This laboratory to 10 MeV. Higher-energy data from Gus85, Yam80, Ped88 and Olsen90.

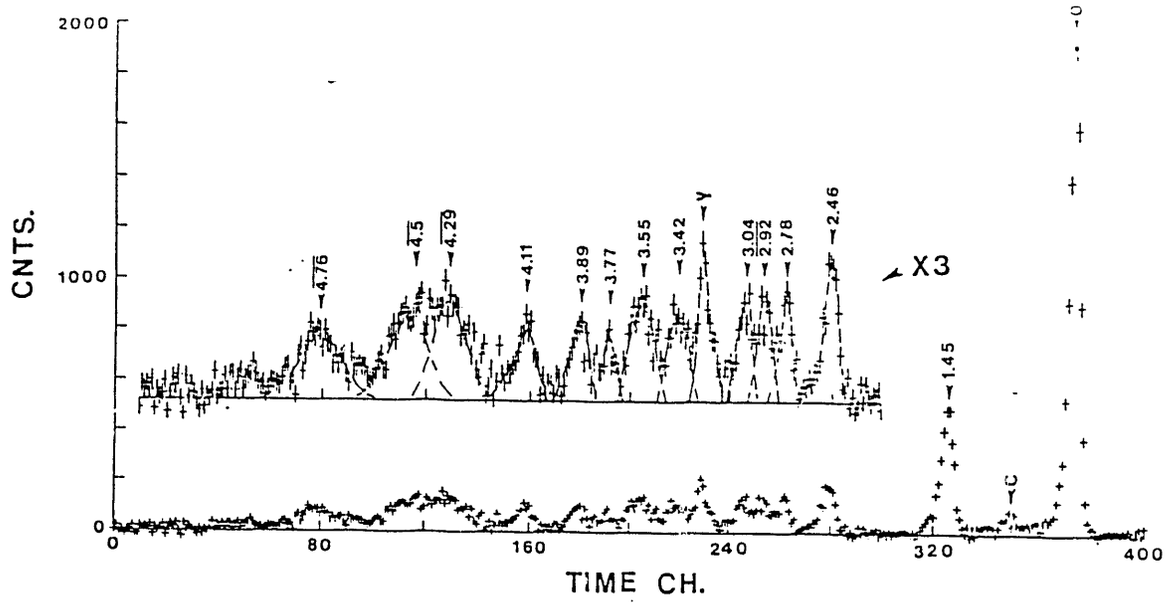

Fig. 3. Measured velocity spectrum at 8 MeV incident energy.

energies, the latter are dominated by compound-nucleus processes, but at higher energies the direct reaction is the governing factor with a strong anisotropy of the scattered neutrons as illustrated in Fig. 4.

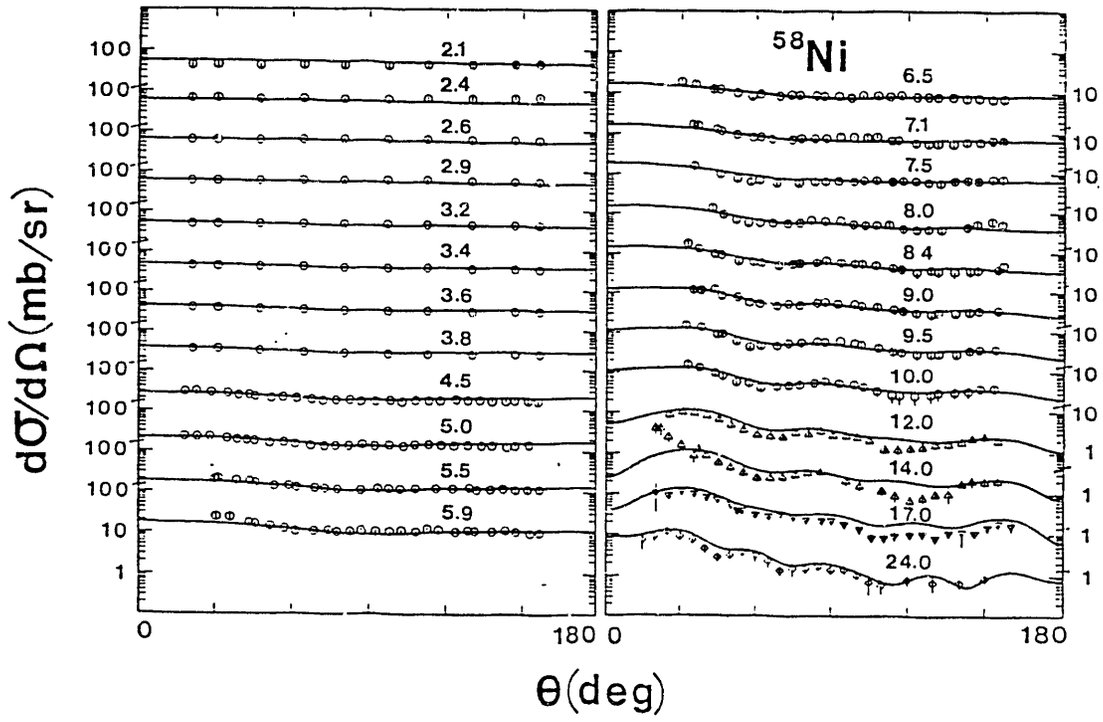

Fig. 4. Inelastic cross sections for the 1.454 MeV level. This laboratory to 10 MeV. Higher-energy results from Gus85, Yam80 and Ped88.

Collectively, the measurements provide a comprehensive data base for applications, model derivation and verification, and for fundamental studies.

MODEL INTERPRETATIONS

The model interpretations followed a graded approach, extending from the simple spherical optical model to progressively more complex models. The model parameters were derived by explicit chi-square fitting of the elastic-scattering data, with concurrent subjective considerations of σ_t and σ_{inel} cross sections, and of the strength functions.

Initially, a simple spherical optical model was derived, suitable for many applications. The model geometry is energy dependent as it must be due to the dispersion relationship. The energy dependence of the real-potential strength generally follows the Hartree-Fock prediction, but there is a pronounced structure at ≈ 5 MeV, as shown in Fig. 5. The imaginary-potential strength falls with energy in a physically unattractive manner. It has been shown that such a

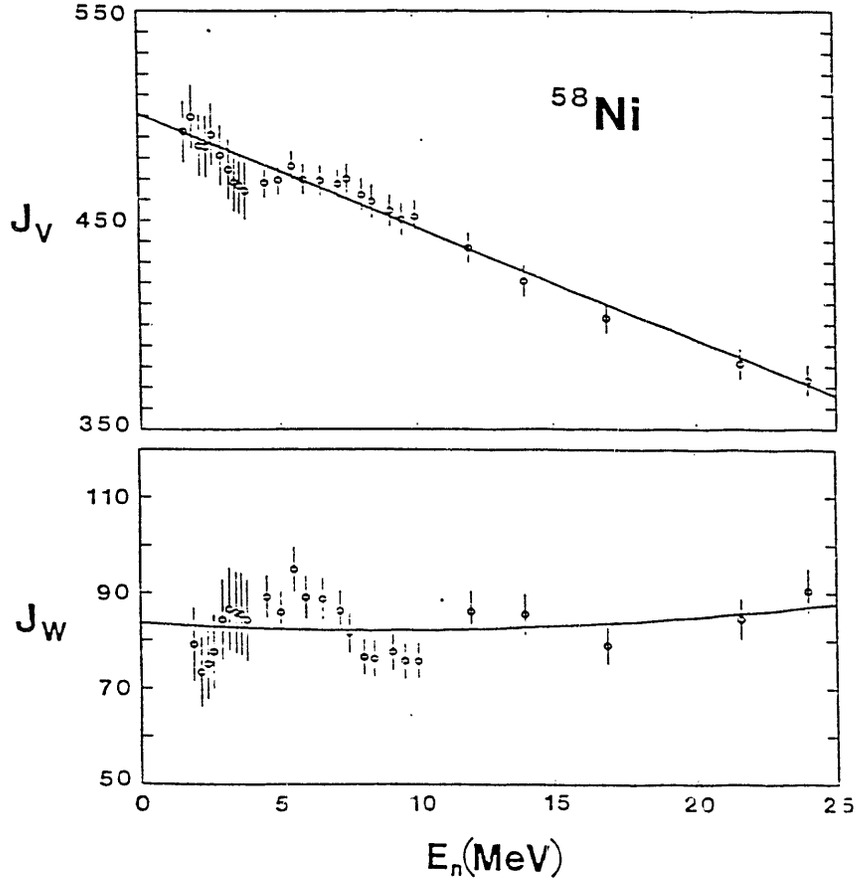

Fig. 5. Real (J_V) and imaginary (J_W) spherical OM strengths in volume-integral-per-nucleon.

behavior is characteristic of a spherical model of a vibrational nucleus [Law87]. The simple spherical model gives a good parameterization of the observed total and elastic-scattering cross sections (see the curves of Figs. 6 and 2, respectively), and an acceptable representation of the strength functions. Further, it has the advantages of simplicity. The obvious shortcomings are; i) physically odd energy-dependencies, ii) failure to describe direct inelastic scattering, and iii) it is devoid of consideration of dispersion or collective effects.

The fundamental dispersion relationship

$$V(r,E) = V_{HF}(r,E) + \frac{P}{\pi}\int_{-\infty}^{+\infty} \frac{W(r,E')dE'}{(E-E')}$$

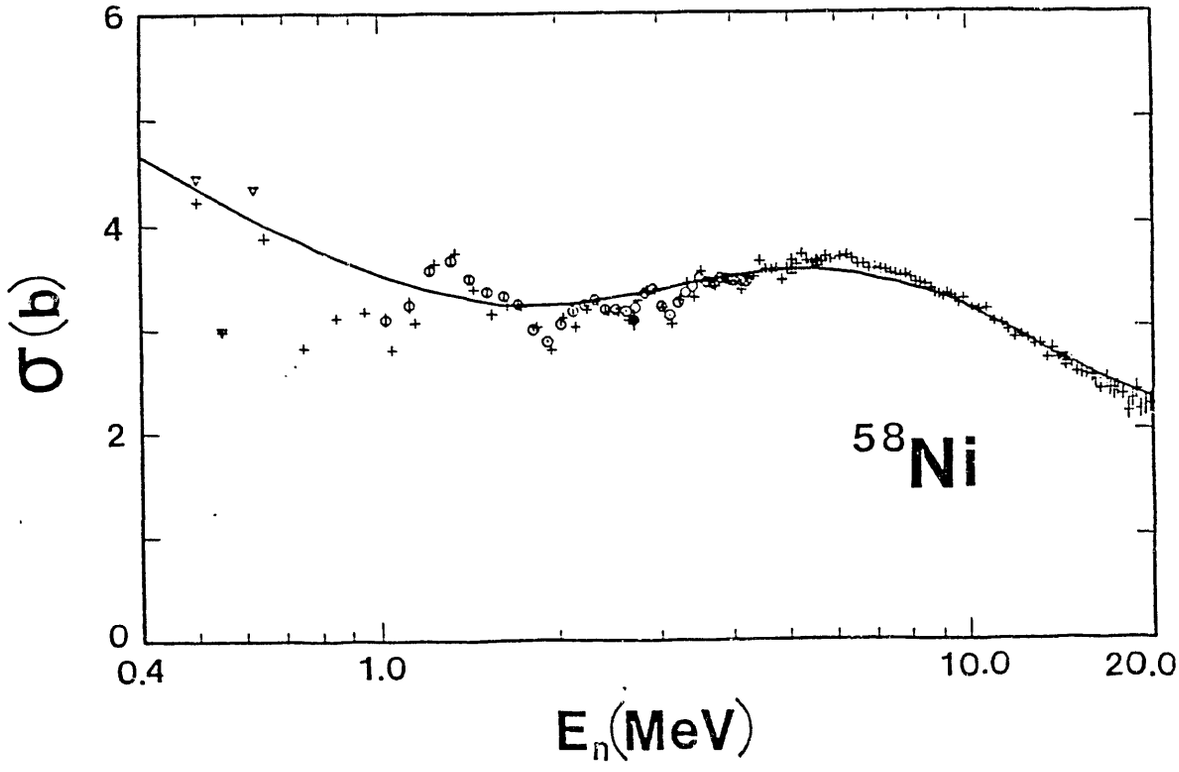

Fig. 6. Energy-averaged σ_t of ^{58}Ni. Symbols indicate experimental results.

couples real and imaginary potentials, and adds a surface component to the Saxon-Woods real potential [Sat83]. The Fermi surface of ^{58}Ni is at large negative energies resulting in a negative surface component of the real potential over the majority of the positive energy domain (see Fig. 7). The entire spherical interpretation was repeated using

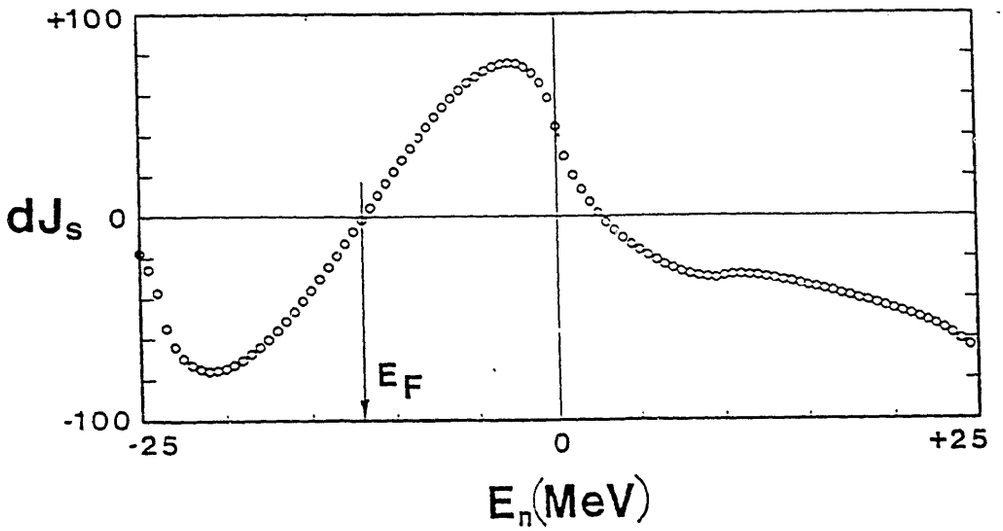

Fig. 7. Surface component of the real-potential strength due to the dispersion relationship (dJ_s).

the dispersion relationship. The resulting potential gave results similar to those of the simple spherical optical model. Some of the energy dependencies of the potential geometries were alleviated (but not removed), and the energy-dependent structure of the real potential remained. In this case, the consideration of the dispersion relationship did not significantly improve on the parameterization of the simple spherical optical model outlined above.

Proceeding to more complex models, it was assumed that ^{58}Ni could be represented as a 1-phonon vibrator, coupling ground and first-excited 1.454 (2^+) MeV states, and β_2 was included in the variable parameters. The assumption is not exactly valid as the quadrupole moment of ^{58}Ni $\neq 0$. With this assumption, the experimental interpretation was repeated. The model geometries remained energy dependent, but the structure in the real-potential strength, evident in the spherical models, was considerably alleviated, as shown in

Fig. 8. Moreover, the imaginary potential strength slowly increases with energy in a physically more acceptable manner. A good

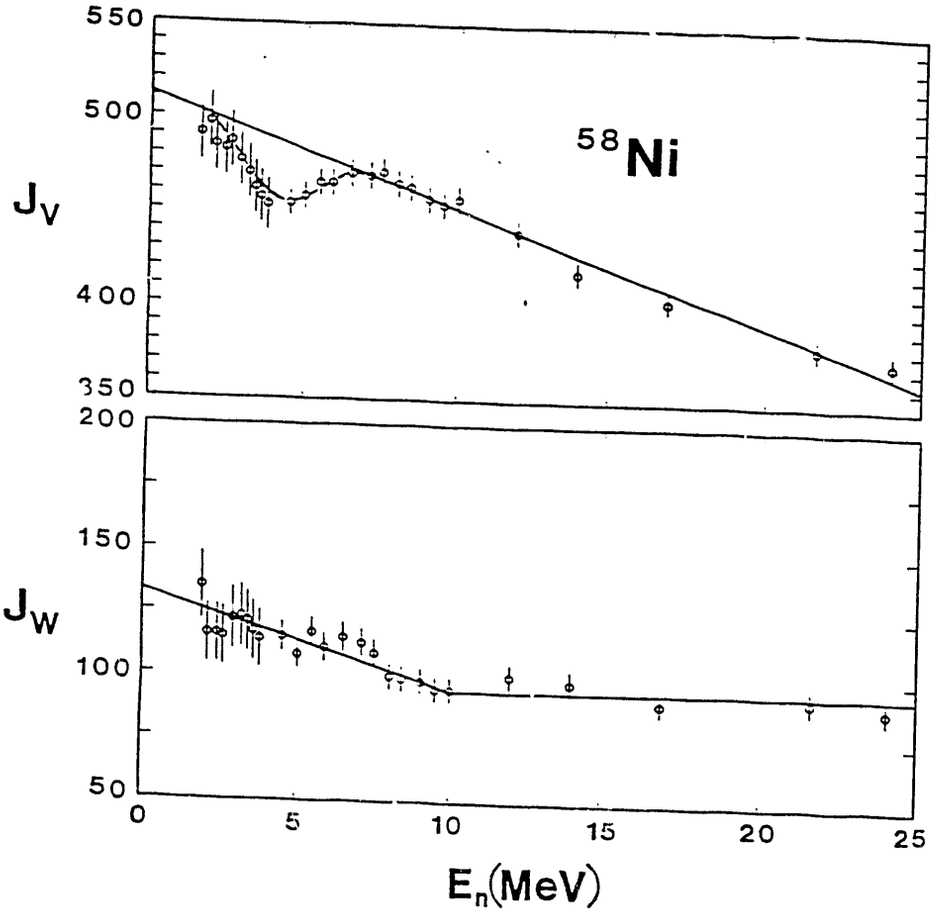

Fig. 8. Real (J_v) and imaginary (J_w) potential strengths obtained with the 1-phonon vibrational model.

description of σ_t and of the elastic scattering (Fig. 9) was retained. In addition, the excitation of the prominent 2^+ level by inelastic scattering is very well described (see the curves of Fig. 4), and the elastic-scattering polarizations were reasonably represented. These results were obtained with $\beta_2 = 0.20 \pm 0.015$, which implies a deformation length of $\delta_{nn} = 0.8948$ at 10 MeV. This value is between the corresponding δ_{EM} of 0.849 and δ_{pp} of 0.9639, as predicted by the core-coupling model [Mad75]. However, one should remember that the deformation length, δ, is a f(R), and R is a f(E) due to the dispersion relationship, and thus the comparisons are meaningful only at specified energies.

Since the 1-phonon model leads to improved results, more complex couplings were considered. Using a 1- and 2-phonon model, results similar to those of the above 1-phonon model were obtained, with a reduction of β_2. There was a small direct-reaction component due to the inelastic-excitation of the 2-phonon states, but not an increase sufficient to greatly improve the agreement between observation and calculation. Moreover, the structure in the real-potential strength

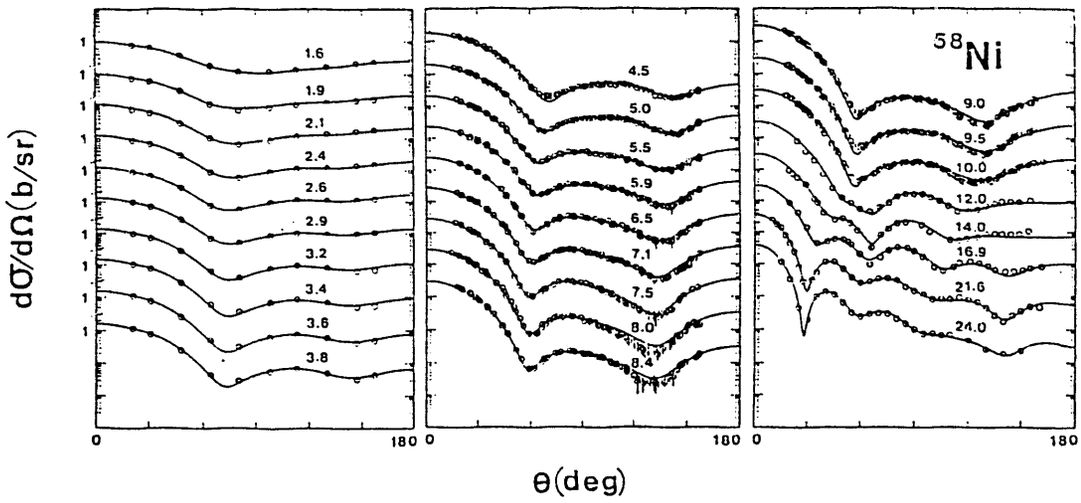

Fig. 9. Measured (symbols) and calculated (curves) elastic scattering cross sections. Calculations used the 1-phonon model.

was not further alleviated. In order to introduce an entirely different coupling of ground and first-excited states, a simple rotational model was examined. The assumption is not particularly physically attractive, but it does grossly change the coupling scheme. The resulting rotational model did not lead to a significant improvement over the more attractive vibrational approaches.

SUMMARY COMMENTS

From this and other Argonne work, a systematic pattern is emerging. The real potential of energy-averaged models is qualitatively global with essentially a constant diffuseness. The real radius is mass and energy dependent, with the latter characteristic not entirely due to the dispersion relationship. Approximately, $r_v = r_0 + r_1/A^{1/3}$, where $r_0 = f(E)$ and r_1 a constant. Furthermore, the real-potential strength follows a simple dependence on isospin and r_v that is consistent with the nucleon-nucleon interaction strength. The imaginary potential is specific to each target, reflecting nuclear structure, collective effects, etc. These characteristics are mildly reflected into the real potential through the dispersion relationship. Elastic neutron scattering is not sensitive to deformation (e.g., to β_2), but inelastic scattering is. Deformation lengths are radii dependent and thus energy dependent. The measurements and associated models of this work should substantively contribute to the provision of data for the design of nuclear-energy systems. However, the collective effects in this region of structural materials are very complex, far more so than accounted for by the models. Thus, there is merit in a search for a more fundamental understanding of a very difficult problem. One approach being explored is the calculation of the neutron interaction from EM matrix elements derived from experimental measurements and/or as estimated from the shell model. This avenue has led to encouraging qualitative results, as illustrated in Fig. 10.

REFERENCES

Detailed references and numerical tables of potential parameters are given in the report ANL/NDM-120, "Fast-neutron Total and Scattering Cross Sections of ^{58}Ni and Nuclear Models", A. Smith, P. Guenther, J. Whalen and S. Chiba (1991).

Har86 J. Harvey, private communication (1986).
Bud82 C. Budtz-Jorgensen et al., Z. Phys. A306 265 (1982).
Gus85 P. Guss et al., Nucl. Phys. A438 187 (1985).
Yam80 Y. Yamanouti et al., NBS-594 (1980).
Ped88 R. Pedroni et al., Phys. Rev. C38 2052 (1988).
Ols90 N. Olsson et al., Nucl. Phys. A509 161 (1990).
Law87 R. Lawson et al., BAPS 32 32 (1987).
Sat83 G. Satchler, "Direct Nuclear Reactions" Clarendon (1983).
Mad75 V. Madsen et al., Phys. Rev. C12 1205 (1975).

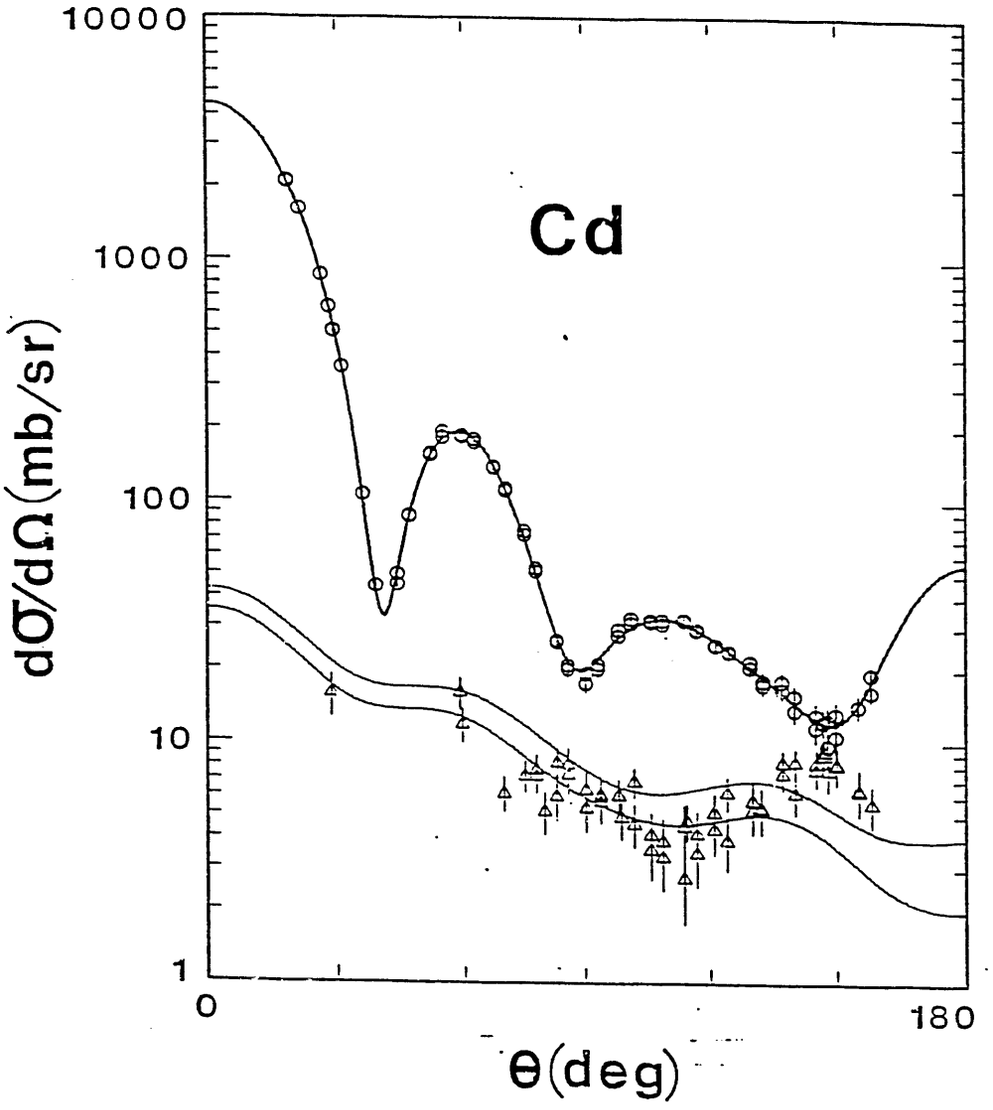

Fig. 10. Measured (symbols) and calculated (curves) scattering cross sections of the even isotopes of cadmium. The upper distribution is due to the elastic and inelastic scattering from the first 2^+ level. The lower distribution is due to the 2^+ excitation alone where the higher curve is obtained using a 1-phonon calculation, and the lower a 3-phonon calculation.

END

DATE
FILMED
01/21/92